2019

Tissue equivalence of diamond for heavy charged particles

Jeremy A. Davis
University of Wollongong, jeremyd@uow.edu.au

Peter Lazarakis
University of Wollongong, peterl@uow.edu.au

James Vohradsky
University of Wollongong, jev720@uowmail.edu.au

Michael L. F Lerch
University of Wollongong, mlerch@uow.edu.au

Marco Petasecca
University of Wollongong, marcop@uow.edu.au

See next page for additional authors

Publication Details

Davis, J. A., Lazarakis, P., Vohradsky, J., Lerch, M. L. F., Petasecca, M., Guatelli, S. & Rosenfeld, A. B. (2019). Tissue equivalence of diamond for heavy charged particles. Radiation Measurements, 122 1-9.

Tissue equivalence of diamond for heavy charged particles

Abstract
A dedicated Geant4 study was developed to determine a correction factor (C) to convert the energy deposition response in diamond to water for heavy charged ions, with atomic number (Z) greater than 2 with energies typical of Galactic Cosmic Rays. The energy deposition response within an ideal diamond based microdosimeter was modelled and converted into a microdosimetric spectrum. The simulation was then repeated, substituting diamond with water. It was shown that by applying the correction factor, the energy deposition and microdosimetric response in diamond could be matched to that of water. The correction factor was determined to be C = 0.32 to 0.33. This study has shown a weak dependence of the correction factor C with respect to the Z of the projectile. The correction factor remains applicable for converting microdosimetric spectra in diamond to water for Galactic Cosmic Rays. This result is extremely encouraging and indicative of the applicability of diamond for use in radioprotection applications in space environments.

Disciplines
Medicine and Health Sciences

Publication Details
Davis, J. A., Lazarakis, P., Vohradsky, J., Lerch, M. L. F., Petasecca, M., Guatelli, S. & Rosenfeld, A. B. (2019). Tissue equivalence of diamond for heavy charged particles. Radiation Measurements, 122 1-9.

Authors
Jeremy A. Davis, Peter Lazarakis, James Vohradsky, Michael L. F Lerch, Marco Petasecca, Susanna Guatelli, and Anatoly B. Rosenfeld

Tissue Equivalence of Diamond for Heavy Charged Particles

Jeremy A. Davis[a,b], Peter Lazarakis[a], James Vohradsky[a], Michael L. F. Lerch[a,b], Marco Petasecca[a,b], Susanna Guatelli[a,b], Anatoly B. Rosenfeld[a,b]

[a] *Centre for Medical Radiation Physics, University of Wollongong, Northfields Avenue, Gwynneville N.S.W 2500, Australia*
[b] *Illawarra Health and Medical Research Institute, University of Wollongong, Northfields Avenue, Gwynneville N.S.W 2500, Australia*

Abstract

A dedicated Geant4 study was developed to determine a correction factor (C) to convert the energy deposition response in diamond to water for heavy charged ions, with atomic number (Z) greater than 2 with energies typical of Galactic Cosmic Rays. The energy deposition response within an ideal diamond based microdosimeter was modelled and converted into a microdosimetric spectrum. The simulation was then repeated, substituting diamond with water. It was shown that by applying the correction factor, the energy deposition and microdosimetric response in diamond could be matched to that of water. The correction factor was determined to be C=0.32 to 0.33. This study has shown a weak dependence of the correction factor C with respect to the Z of the projectile. The correction factor remains applicable for converting microdosimetric spectra in diamond to water for Galactic Cosmic Rays. This result is extremely encouraging and indicative of the applicability of diamond for use in radioprotection applications in space environments.

Keywords: Microdosimetry, diamond, tissue equivalence, Geant4, heavy charged ions.

1. Introduction

Heavy charged ions (HZE) such as carbon and oxygen constitute a small (≈1% total flux) but significant component of Galactic Cosmic Rays (GCR) [1] (see Fig. 1) due to a higher radiobiological effectiveness (RBE). The renewed interest in manned space missions and exploration of the solar system requires an increased understanding and use of microdosimeters for quantifying the effect of HZE in human tissues. Likewise, it is important in the context of radioprotection in space, to be able to quantify the effect of HZE in human tissues and monitor the radiation exposure of astronauts over time and provide warning of changes within the radiation environment [2].

The microdosimetric methodology considers the stochastic energy deposition in sensitive volumes with sizes typical of a cell nucleus (≈1-2 μm) and is an effective tool for radioprotection applications in space. Key to microdosimetry is the accurate determination of the *lineal energy (y)* which is defined as the quotient of an energy deposition event (ϵ) and the *mean chord length (l)* of the sensitive volume (SV) [3]. Microdosimetric spectra are typically plotted in a semi-logarithmic scale as events span orders of magnitude. The two most commonly used microdosimetric spectra are frequency ($yf(y)$ vs. $log(y)$) and dose ($yd(y)$ vs. $log(y)$) distributions, where equal areas under the curves represent equal fractions of events and fractional doses, respectively. The experimental determination of these quantities then requires detectors with accurately defined micron sized SVs with known geometry and composition.

In order to investigate the radiation effect in tissue, the detector should ideally be comprised of a tissue equivalent material. A material is said to be tissue equivalent if the scattering/absorption interactions are comparable to that within tissue, such that the absorbed dose within the media is representative of the dose

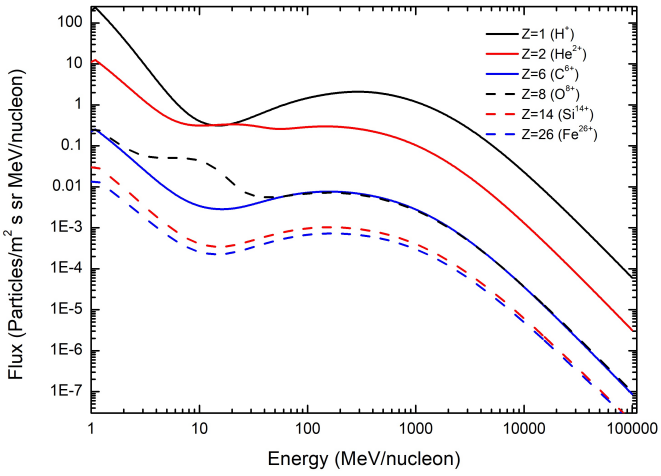

Figure 1: Differential spectra for GCR proton, alpha and HZE particles with Z >2. Data derived from CREME96 at solar minimum at 1AU [1].

absorbed within tissue in the radiation environment of interest, i.e. independent upon ion/photon energy. An important parameter in the context of tissue equivalence is that of the effective atomic number of the target (Z_{eff}) given the well known dependence of electromagnetic interactions upon Z, where elements with similar Z will respond similarly to radiation of a specific energy/type [4]. The parameter Z_{eff} arises given the composite nature of many materials, to allow for a theoretical determination of photon based interactions that would occur for a composite material containing two or more elements of different Z over some given energy range. Z_{eff} is widely used to denote the tissue equivalence of materials for dosimetry or determine an unknown material in medical imaging. In microdosimetry, the problem is more complex than simply considering the effective atomic number of the target material given the contamination of charged particle secondaries. Thus it becomes more and more necessary to consider the stopping power within the target medium, i.e, dE/dx. This is increasingly relevant in radioprotection applications in space, in which the mixed radiation field consists of a veritable zoo of charged particles with a wide range of energies.

The tissue equivalent proportional counter (TEPC) is the gold standard in microdosimetry for radioprotection applications in space [5, 6]. The primary advantage of the TEPC is in its spherical geometry which allows for isotropic response due to incident radiation, particularly useful in the complex radiation environment of space.The TEPC is filled with a low pressure tissue equivalent gas to simulate 1μm of biological tissue. It is reliant upon the assumption that the radiation field incident upon the SV of the TEPC is equivalent to that incident upon a biological cell. However, the high voltage operation, limited spatial resolution, wall-effects and the technical difficulties in constructing 2D arrays of SVs hamper the use of TEPCs in particular applications. One of the leading alternatives to the TEPC is the solid state Silicon-On-Insulator (SOI) microdosimeter developed at the Centre for Medical Radiation Physics (CMRP), University of Wollongong, Australia and the solid state microdosimeter based on a monolithic silicon telescope developed by the Istituto Nazionale di Fisica Nucleare (INFN) in collaboration with ST-Microelectronics of Italy [7, 8, 9]. The two leading SOI microdosimeters thus far, are the Bridge and Mushroom detectors [10, 11]. These devices have

the capability for real-time measurement of lineal energy and determination of RBE for therapeutic carbon ion beams [12, 13]. However, being composed of silicon, these devices are inherently non-tissue equivalent. Diamond is often considered as being a more tissue equivalent material than silicon for photons, given the close proximity in the effective atomic numbers of carbon (Z=6) compared to silicon (Z=14) with the effective atomic number of water (Z_{eff}=7.42) and soft tissue (Z_{eff}=7). Whilst there is certainly an argument for the use of diamond in dosimetric applications based upon its tissue equivalence, its applicability has been hampered by its lower sensitivity, i.e. energy required to create an electron hole pair ($E_{e/h}$=3.6eV and 13eV for silicon and diamond, respectively [14]). The lower sensitivity of diamond in comparison with Silicon is leading to increasing of the thickness of SV to extend dynamic range of microdosimeter, which would likely lead towards an increased contribution of stoppers, which affects the microdosimetric spectrum. Another important parameter in terms of tissue equivalence especially in the case of positively charged particles, is the restricted linear collision stopping power (also referred to as linear energy transfer (LET)) and is proportional to Z/A [15, 16]. Essentially it is a measure of localised energy loss due to coulomb interactions with atomic electrons and nuclei of the target and thus highly dependent upon the target material (Z_{eff}, A_{eff} and ρ) [4].

It was shown in a previous study [17], that given an appropriate correction factor (C) based upon scaling the spatial dimensions of a sensitive volume (SV) of interest, the energy deposition response in diamond could be converted (C=0.32) to that in water for protons and alpha particles, for energy range 10 $\mathrm{MeV} < E_K < 1$ GeV. This correction factor is based upon the ratio of mass stopping power (SP) of an ion within diamond to water, and hence has a direct correlation to the dimensions of the SV. For protons and alpha particles in diamond, this ratio is relatively constant between 1 MeV and 10 GeV. The stability in the correction factor for protons and alpha particles previously determined is owed to this constancy of the SP ratio. The correction factor can be written as:

$$C = \frac{SP_{Water}}{SP_{Diamond}} = \frac{SS_{Diamond}}{SS_{Water}}$$

where SS_{Water} and $SS_{Diamond}$, are the linear dimensions or Side Sizes (SS) of the water and diamond cubic SVs, respectively. Theoretically, as long as the number of recoils within the SV due to nuclear interactions is not significant, i.e. having a impact upon the energy deposition spectra and the SP ratio depicted for protons in Fig. 2 remains constant for ions with $Z > 2$ for the energy range of interest, so too, will the diamond to water correction factor C. It should be noted that this correction factor C has an inherent assumption that the geometry/shape of the SV of interest remains constant and that only the spatial dimensions are scaled.

This work is performed by means of Geant4 simulations. The goal of this work is to determine if the previously determined correction factor for protons and alpha particles can be applied for incident heavy charged ions with Z>2, i.e., Carbon, Oxygen, Silicon and Iron nuclei. Additionally, Geant4 will be used to determine the mean chord length for the 2nd Generation 3D-LES [20] diamond microdosimeter. Accurate determination of the mean chord length is necessary to calculate more accurately the lineal energy spectra, however it is reliant in this case upon the a-priori assumption of the SV dimensions. To address this, a model of the diamond microdosimeter has been modelled in Synopsys TCAD to determine the real dimensions of the SV and compare them to the ones adopted in the Geant4 simulation study. The SV dimensions will be assessed in terms of charge collection isolation/confinement. This model will be used as proof of concept to validate the technology prior to experimental investigation. Lastly, using the aforementioned mean chord length, the correction factor will be used to convert the microdosimetric response within the current state of the art diamond microdosimeters to that of water for the GCR spectrum for radioprotection in space applications. This work will be directly applicable for Solar Particle Events (SPE) given the similar energy

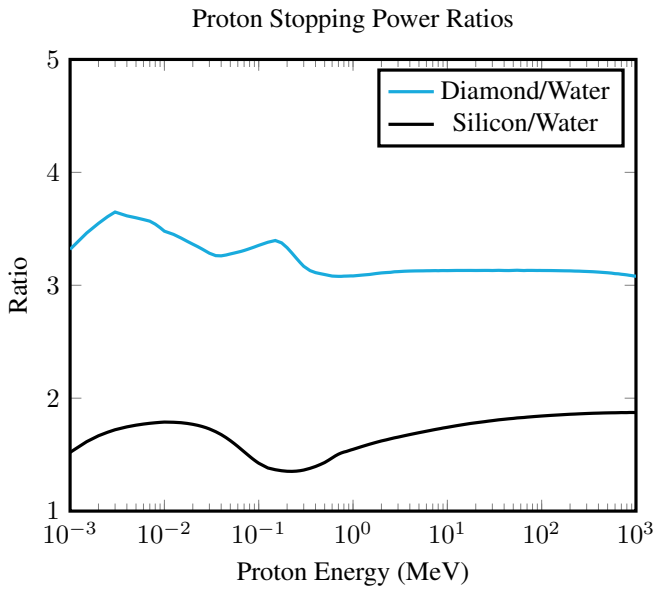

Figure 2: Stopping power ratios for protons in diamond/water and silicon/water for proton energies between 1 keV and 1 GeV [18] [19].

range to GCR (even though their spectrum is dominated more by lower energy particles) as well as heavy ions used in Heavy Ion Therapy (HIT) which have energies up to ≈400 $\mathrm{MeV\,u^{-1}}$ [12].

2. Geant4 Simulation Study

A dedicated Geant4 application (version 10.01) [21] [22] was developed for this study to calculate the energy deposition distributions deriving from incident Carbon, Oxygen, Silicon and Iron ions within a diamond microdosimeter SV. The Geant4 Low Energy Physics Package, based on Livermore data libraries [23] [24], was selected to describe all the electromagnetic interactions of particles, down to 250 eV. The Geant4 QGSP_BIC_HP physics list was selected to model the hadronic physics processes because it has shown the best agreement with experimental results for the energy range of interest in this work [12]. The simulation-based study allows investigating the effect of nuclear recoils deriving from hadronic interactions upon the tissue equivalence of diamond. Primary and secondary particles were tracked in the experimental set-up and the output of the simulation was the energy deposition per event in the SVs, where one event corresponds to the generation of one primary particle and its associated secondary particles. The Geant4 simulation study is carried out in two parts, firstly the determination of the correction factor for bare diamond SVs, without contacts and packaging, for monoenergetic heavy ions and secondly the evaluation of this correction factor for a fully modelled diamond microdosimeter when exposed to the mixed isotropic radiation field typical of GCR.

2.1. Correction Factor for HZE

A cubic SV (10x10x10 $\mu\mathrm{m}^3$) of diamond was modelled in free space, i.e. within a vacuum. Heavy charged ions modelled using the Geant4 General Particle Source, were defined to be normally incident upon

the SV as a pencil-beam. The following ion species were chosen for use in this study: Carbon, Oxygen, Silicon and Iron as they are significant components of the GCR HZE radiation field. For each ion species modelled, several different monoenergetic energies were selected, from: 10 $\mathrm{MeV\,u^{-1}}$, 50 $\mathrm{MeV\,u^{-1}}$, 125 $\mathrm{MeV\,u^{-1}}$, 250 $\mathrm{MeV\,u^{-1}}$, 500 $\mathrm{MeV\,u^{-1}}$ and 1 $\mathrm{GeV\,u^{-1}}$ in order to cover the majority of the energy range for GCR. 10^7 events were generated in each simulation to obtain statistically meaningful results. Energy deposition events occurring within the SV are recorded and plotted in a histogram. The diamond SV is then replaced with water and the spatial dimensions increased until the energy deposition distribution is equivalent to the one in a diamond SV. The agreement is determined by means of statistical analysis with MATLAB [25].

2.2. Diamond Microdosimetry in Free Space

In the second part of the study, a realistic model of microdosimeter device (instead of simply modelling the cubic SV as described in Section 2.1) was modelled in the simulation study. The diamond microdosimeter features an array of cylindrical electronic grade diamond SVs (white) with diameter 30µm and height of 10µm, as shown in Fig. 3 and 4. At the centre of each SV is a cylindrical 'inner' electrode structure of silver (Grey). Likewise, each SV is surrounded by a cylindrical shell of silver with inner diameter of 30µm and outer diameter of 40 µm to represent the 'outer' electrode structure. The 'outer' electrode of each SV is connected to its nearest neighbour SV by a 40µm long silver bridge with width and depth of 5µm, so as to create rows of SVs connected in parallel. Likewise, the 'inner' electrode structure of each SV is connected in parallel with aluminium strips (red), surrounded by PMMA (blue) as depicted in Fig. 3. The SV array is situated above a 2µm thin layer of boron doped diamond (green) atop a 300µm thick substrate of low grade diamond (yellow). The diamond SVs have been substituted with water SV with appropriately scaled dimensions (diameter =30µm $\div$ C, height =10µm $\div$ C) to provide equivalent energy deposition spectra to the diamond device. The pitch between diamond SVs was also adjusted using the correction factor, whilst the size of all non diamond components remained constant in this study.

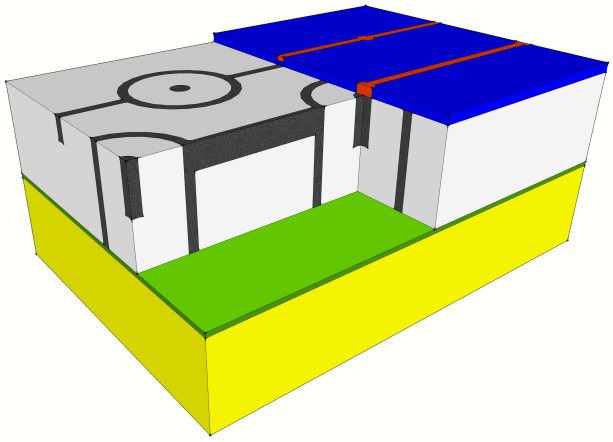

Figure 3: Subsection of the diamond microdosimeter prototype featuring cylindrical sensitive volume structures modelled in Geant4.

In this study, the isotropic field of GCR is simplified such that it is comprised of protons (90.926%), alpha particles (6.568%), Carbon (0.222%), Oxygen (0.228%), Silicon (0.032%) and Iron nuclei (0.024%), weighted to give 100% [1]. The isotropic radiation field is defined to be incident upon the diamond microdosimeter and the energy deposition within each SV is recorded.

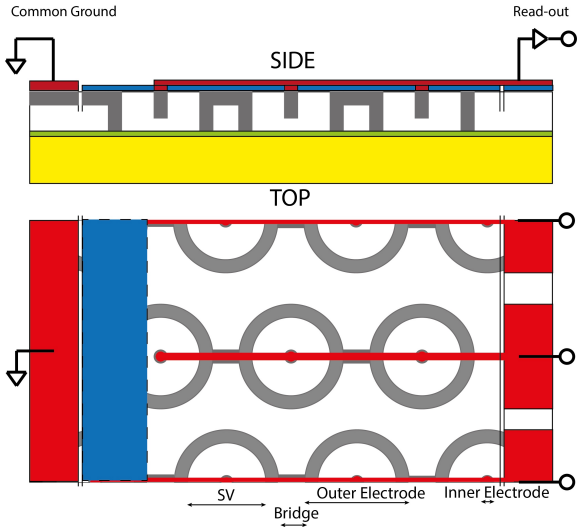

Figure 4: Top- Cross section of device. Bottom- Birds eye view of device.

Given the relatively complex nature of the SV shape due to the presence of the inner electrode, an additional simulation study was performed to determine the chord length distribution and thus the mean chord length (l) for the cylindrical SV. This study records the track length of an isotropic field interaction-less 'Geantinos' as they traverse the diamond SV. The SV is modelled without any contacts and packaging.

Using the energy deposition (ϵ) spectrum and the previously determined mean chord length (l) the result is converted to a microdosimetric spectrum and compared against an equivalent detector comprised of water and with appropriately scaled SVs by means of C. This study provides an evaluation of the appropriateness of the correction factor C, calculated following the methodology described in section 2.1, for mixed radiation fields as well as providing a means to assess the geometry of the diamond SVs in terms of microdosimetric applications. This assessment of the geometry will be performed in terms of the contribution to the microdosimetric spectrum of 'crossers' and 'stoppers'.

2.3. Analysis

The two sided Kolmogorov-Smirnov (KS) test was used to quantify the agreement between distributions derived from different data sets [26] [17]. The KS test is a goodness of fit statistics test, which analyses the maximum vertical distance between the cumulative frequency distribution of each data-set F_1 and F_2, as shown Equation 1.

$$max\left(\left|F_1\left(x\right) - F_2\left(x\right)\right|\right) \tag{1}$$

The KS test output is known as a p-value, representing the test of the null hypothesis that the two compared energy deposition distributions are compatible. The best agreement between spectra will be established by results with the highest p-value, resulting from the statistical comparison of the energy deposition spectra, in the diamond and in the water microdosimeter sites, by means of the Kolmogorov-Smirnov test.

An additional measure of the appropriateness of the scaling factor to convert the response in diamond to that of water in the context of microdosimetry is also presented in this work. This alternative method relies upon the use non-stochastic microdosimetric quantities/expectation values, i.e., frequency mean lineal

energy (y_F), dose mean lineal energy (y_D) and the saturation-corrected dose-mean lineal energy (y^*) and are defined in equations 3, 2 and 4 [3]. The hypothesis of this form of analysis is that the quantities as determined for diamond and water based devices should agree if the correction factor is appropriate.

$$\bar{y}_F = \int_0^\infty y.f(y)dy \tag{2}$$

$$\bar{y}_D = \int_0^\infty y.d(y)dy = \frac{1}{\bar{y}_F}\int_0^\infty y^2.f(y)dy \tag{3}$$

$$\bar{y}_* = \frac{y_0^2 \int_0^\infty \left(1 - exp(-y^2/y_0^2)\right) f(y)dy}{\int_0^\infty y.f(y)dy} \tag{4}$$

3. TCAD Simulation Study

3.1. Charge confinement for cylindrical sensitive volumes

The diamond microdosimeter was modelled using Synopsys Technology Computer Aided Design (TCAD) software. A 2D model of the device was designed to represent a cross-section of the device, taken through the center of three SVs. The model was designed to include all of the relevant/pertinent features i.e., inner/outer and bridge electrode structure, intrinsic diamond, electrical active p-type diamond (boron doped) and low quality (nitrogen rich) substrate. A box method meshing strategy was utilised in this study. In regions of interest, i.e. metal/diamond interfaces or ion strike regions, the meshing strategy was optimised such that finer mesh elements were applied.

The model makes use of the Device Simulation for Smart Integrated Systems (DESSIS) code which is part of Synopsys TCAD package. The DESSIS toolkit solves the transient Poisson equation and electron and hole continuity equations for the diamond device. The model implemented includes essential models to describe the physics of the charge transportation and ion interaction within the device. The doping dependent Shockley-Read-Hall physics model, was employed to describe carrier generation and recombination in terms of the appropriate carrier continuity equations. The mobility model specified was utilized to take into account carrier scattering via ionised impurities, saturation of carrier velocity in regions of high electric fields and the potential for mobility degradation due to scattering driven by surface roughness.

Given the charge injection and built-in potential properties of the p-type interface layer that acts not only as a common electrode but also to electrically confine the SV structure, the device will likely operate in passive mode. However it has also been shown in previous study that CCE within diamond is bias dependent and saturates around 1 $\mathrm{V\,\mu m^{-1}}$ [20, 27]. To that end, the common outer electrode was grounded, whilst a bias of 10 V was applied to the inner electrodes. Read-out was performed at the inner electrode.

The numerical parameterisation of diamond as a material in multivariate physics tool-kits is a relatively new area. However, with the ever increasing interest in this material, the amount of experimental data on offer has made it increasingly easier to validate material parameter files (.par) to model the physical behaviour of diamond [28] [29]. Currently, Diamond.par is not a standard parameter file within the Synopsys TCAD package. Due to this lack, a model of polycrystalline diamond developed by the University of Perugia and described by Morozzi, et al, 2016 was used to describe the diamond material modelled in this work [30].

The HeavyIon model was used to simulate a hit by a minimum ionizing particle (MIP), with perpendicular tracks passing through the device and generating a continuous charge distribution that drift toward the electrode in the presence of an electric field. In the case of diamond, the Linear Energy Transfer (LET) of the MIP was defined to be 5.8x10^{-8} $\mathrm{pC\,\mu m^{-1}}$, i.e. 36 electron hole pairs per micrometre. The device

models were used to investigate the charge confinement of the device by assessing the Charge Collection Efficiency (CCE) of the device for various strike positions inside (x=5 μm) and outside (x=40 and 100 μm) the cylindrical sensitive volume structures. The aim of this study was to confirm the hypothesis that charge collection is confined by the cylindrical electrode structure and validate the mean chord length previously discussed. The CCE was defined as:

$$CCE = \frac{Q_(x)}{Q_(x = 10)} * 100 \tag{5}$$

Where $Q_(x)$ is the charge collected by an electrode (Common Outer electrode). Charge collection in this study is defined as the integral of the TotalCurrent over the simulated time frame multiplied by the total time. The CCE for each strike is normalised to strikes occurring within the central SV structure (i.e. x=10 μm) in order to determine relative response as defined by Equation 5.

4. Simulation results: Correction Factor for HZE

This section summarises the results obtained with mono-energetic pencil beams of Carbon, Oxygen, Silicon and Iron ions with energies spanning from 10 $\mathrm{MeV\,u^{-1}}$ up to 1 $\mathrm{GeV\,u^{-1}}$. An example of the typical output of the simulation study is presented in Fig 5, which details the energy deposition due a 10 $\mathrm{MeV\,u^{-1}}$ carbon ion beam within diamond and water cubic SVs. Table 1 reports the summary of the analysis results for each ion/energy investigated.

The KS GoF test shows that a water SV with SS between 30 and 31 μm shows the best agreement with the energy deposition spectra in a diamond SV with linear SS of 10 μm. The results indicate a slight energy dependence in the correction factor with 0.4 μm increase in the linear SS from 10 $\mathrm{MeV\,u^{-1}}$ to 1000 $\mathrm{MeV\,u^{-1}}$ ions regardless of the ion species. Additionally, whilst not large enough to be statistically significant, there does appear to be some small dependence upon the Z of the incident ion in the level of agreement.

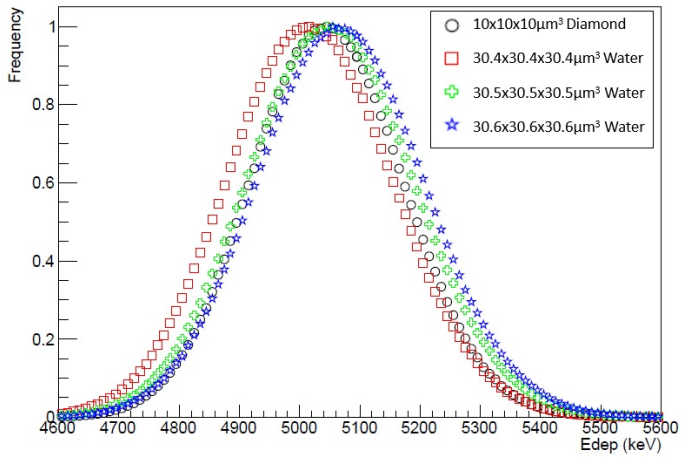

Figure 5: Energy deposition spectra derived from 10 $\mathrm{MeV\,u^{-1}}$ carbon ions incident on diamond and water SVs. The SS of the water SV is indicated in the legend.

Table 1: Summary of Kolmogorov-Smirnov test for analysis of best fit for energy deposition spectra in diamond to water for Carbon, Oxygen, Silicon and Iron ions with energies typical of GCR. The Correction factor C is reported to two decimal places. For brevity, the best fit refers to the dimensions of one side of the cubic water SV which demonstrated the best agreement with energy deposition in the cubic diamond SV with dimensions 10 µm x 10 µm x 10 µm.

Ion (Z)	**Energy** ($\mathrm{MeV\,u^{-1}}$)	**Best agreement in terms of linear SS** ($\mu\mathrm{m}$)	**P-value**	**Correction Factor**
6	10	30.4	0.964	0.33
6	50	30.6	0.932	0.33
6	125	30.6	0.999	0.33
6	250	30.6	1.000	0.33
6	500	30.6	1.000	0.33
6	1000	30.8	0.999	0.32
8	10	30.6	0.999	0.33
8	50	30.6	0.951	0.33
8	125	30.6	0.998	0.33
8	250	30.6	1.000	0.33
8	500	30.6	1.000	0.33
8	1000	30.6	0.997	0.33
14	10	30.6	0.995	0.33
14	50	30.6	0.882	0.33
14	125	30.6	0.944	0.33
14	250	30.6	0.998	0.33
14	500	30.6	0.983	0.33
14	1000	30.8	0.966	0.32
26	10	30.4	0.964	0.33
26	50	30.8	0.271	0.32
26	125	30.6	0.999	0.33
26	250	30.6	0.969	0.33
26	500	30.6	0.823	0.33
26	1000	30.8	0.835	0.32

5. Simulation results: Diamond Microdosimetry in Free Space

The chord length distribution for the cylindrical SV structure is depicted in Fig. 6. The dominant peak at $10\mu\mathrm{m}$ represents the most probable chord length for a traversing particle in an isotropic radiation field, which is unsurprising given the SV dimensions. It should be noted that this determination of the mean chord length of the diamond and water SVs takes the presence of the inner electrode into account. The mean chord length

of the diamond SV was determined to be l_D=11.34µm. The mean chord lengths was likewise determined for the spatially corrected water SVs. For C=0.32, the mean was determined to be l_W=37.28µm, and for C=0.33, the mean chord length was determined to be l_W=36.15µm. Using the aforementioned mean chord lengths the microdosimetric spectra resulting from GCR interactions were determined for both the diamond microdosimeter and its water based counterpart.

In Fig. 7 the total microdosimetric spectra from an isotropic radiation field comprised of GCR hydrogen, helium, carbon, oxygen, silicon and iron ions respectively is presented. The contribution of each ion to the total microdosimetric spectra is presented in Fig. 8 and 9. Two peaks are clearly distinguishable in Fig. 7 at approximately 25 and 100 keV µm^{-1}. These two peaks are primarily the result of proton and alpha energy deposition interactions within the diamond material, see Fig. 8 and 9.

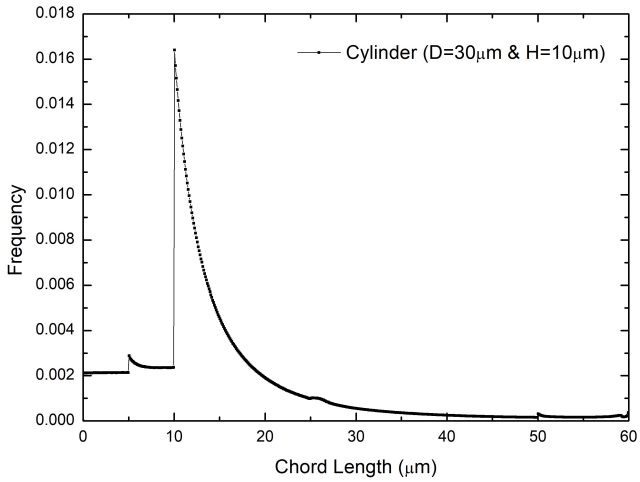

Figure 6: Chord length distribution for the cylindrical SV structures (Diameter=30µm and Height=10µm) of the diamond microdosimeter. Note: this accounts for the effect due to the presence of the inner electrode.

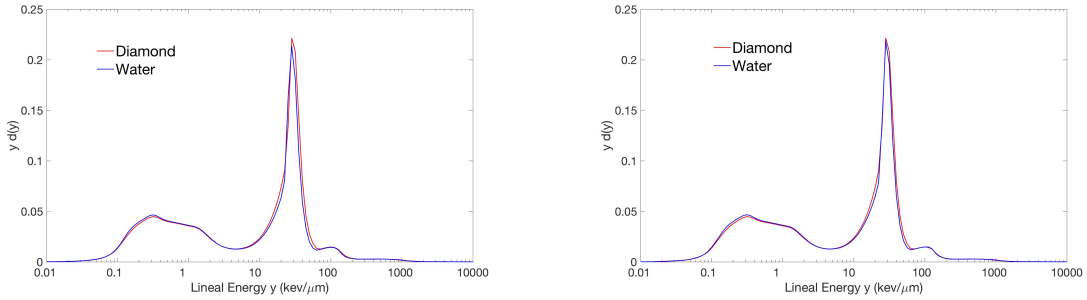

Figure 7: Comparison of the microdosimetric spectrum for diamond (red) and a scaled water (blue) based microdosimeter due to an isotropic field of GCR. Two different correction factors are compared, C=0.32 (left) and C=0.33 (right).

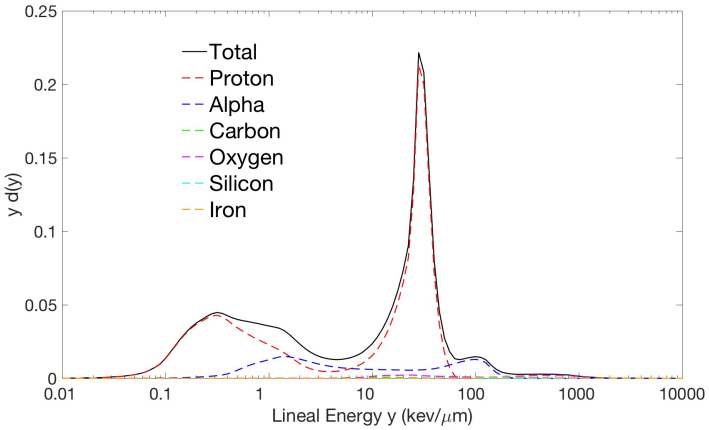

Figure 8: Contribution to the microdosimetric spectrum for the diamond microdosimeter deriving from each GCR nuclear species. The contribution deriving from the different species of incident particles is indicated in the legend.

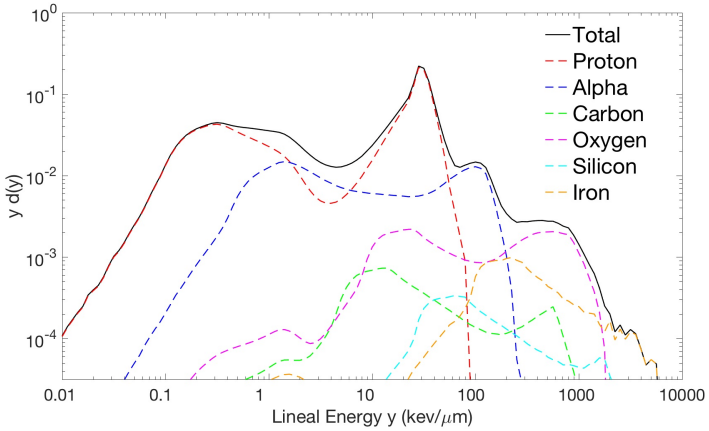

Figure 9: Contribution to the microdosimetric spectrum for the diamond microdosimeter deriving from each GCR nuclear species in log-log scale. The contribution deriving from the different species of incident particles is indicated in the legend.

Table 2 is a summary of the analysis performed upon the microdosimetric spectrum in a diamond and its water based counterpart microdosimeters. The agreement between the two spectra is characterised by the KS test p-value which is performed on an ion by ion basis as well as for the total spectrum, i.e. the weighted contribution of each ion species. The overall agreement as determined by the KS test is the same for C=0.32 and C=0.33, although on an ion by ion basis there is a slight improvement in the case of C=0.33. With the exception of Iron, good agreement between the ion interactions within the water and diamond SVs is found. In the case of Iron, acceptable agreement between the microdosimetric spectrum in diamond and water is improved by imposing a lower limit of 30 $\mathrm{keV\,\mu m^{-1}}$. Without this limit, the KS test p-values for Iron for C=0.32 and C=0.33 are 0.4652 and 0.6789, respectively.

Table 2: Summary of Kolmogorov-Smirnov test for analysis of microdosimetric spectrum of isotropic field of GCR in diamond microdosimeter.

GCR Ion	**GCR weighting (%)**	**P-value (C=0.32)**	**P-value (C=0.33)**
Hydrogen	90.926	0.9999	1.0000
Helium	6.568	0.9848	1.0000
Carbon	0.222	0.9999	1.0000
Oxygen	0.223	0.9979	0.9999
Silicon	0.032	0.9472	0.9472
Iron	0.024	0.9817	0.9952
Total	100	0.9979	0.9979

Whilst the KS test provides a means of characterising the goodness of fit between the two data-sets, it does not provide any quantitative measure, relevant to microdosimetry as to the applicability of a correction factor. To that end, the dose-mean lineal energy (y_D), the frequency-mean lineal energy (y_F) and the saturation-corrected dose-mean lineal energy (y^*) for both diamond and water based microdosimeters are presented. Note: The saturation parameter, y0, has been set to 150 $\mathrm{keV\,\mu m^{-1}}$. These parameters are presented to two decimal places for the total spectrum (see Table 3) as well as for each ion species studied in this work.

Table 3: Microdosimetric parameters (y_D, y_F and y^*) for the microdosimetric spectrum in the diamond and spatially corrected water based microdosimeters for total spectrum . Two different correction factors are considered in this work (C=0.32 and C=0.33). The level of agreement is quantified in terms of a percentage difference.

Parameter	**Diamond**	**Water (C=0.32)**	**Difference**	**Water (C=0.33)**	**Difference**
y_D	28.66 $\mathrm{keV\,\mu m^{-1}}$	29.05 $\mathrm{keV\,\mu m^{-1}}$	1.34%	29.54 $\mathrm{keV\,\mu m^{-1}}$	2.88%
y_F	0.69 $\mathrm{keV\,\mu m^{-1}}$	0.64 $\mathrm{keV\,\mu m^{-1}}$	7.81%	0.64 $\mathrm{keV\,\mu m^{-1}}$	7.81%
y^*	18.23 $\mathrm{keV\,\mu m^{-1}}$	17.08 $\mathrm{keV\,\mu m^{-1}}$	6.73%	17.44 $\mathrm{keV\,\mu m^{-1}}$	4.53%

The results presented in Table 3 demonstrate the importance of choosing the appropriate parameter in order to evaluate the similarities in microdosimetric spectrum in diamond and water microdosimeters. For a correction factor of C=0.32, the choice of the the dose-mean lineal energy (y_D) gives excellent agreement (1.34%) between the diamond and water microdosimetric spectrum. If instead the the frequency-mean lineal energy (y_F) or the saturation-corrected dose-mean lineal energy (y^*) is chosen, the percentage difference becomes more significant, i.e., 7.81 and 6.73%, respectively. For a correction factor of C=0.33 which overall showed better agreement for the previous monoenergetic study, the percentage difference for the dose-mean, frequency-mean and saturation-corrected dose mean becomes 2.88, 7.81 and 4.53% respectively. It is clear then that the choice of non-stochastic microdosimetric criteria such as:y_D, y_F and y^* can have a significant effect upon determining agreement between microdosimetric spectrum.

The contribution for crossing and stopping particles is shown in Fig. 10. The percentage contribution by crossers and stoppers was determined to be 98.3 and 1.7%, respectively, in the case of the diamond

microdosimeter, and 99.1 and 0.9% for the water equivalent counterpart. It is clearly evident that for SVs with diameter of 30 µm and height 10 µm, the contribution of stoppers whilst relatively small with respect to that of the crossers is clearly an issue with regards to the microdosimetric method. This requires changes to the SV dimensions and thus the chord length distribution which is depicted in Fig. 6. It is possible to infer that the current design should be improved (smaller SVs) in order to be applicable for microdosimetry in space, given the large contribution of energy deposition due 'stoppers' to the total spectra. However, it is possible to use this design as a base line in which to define an ideal diamond based microdosimeter for radioprotection applications in a space environment.

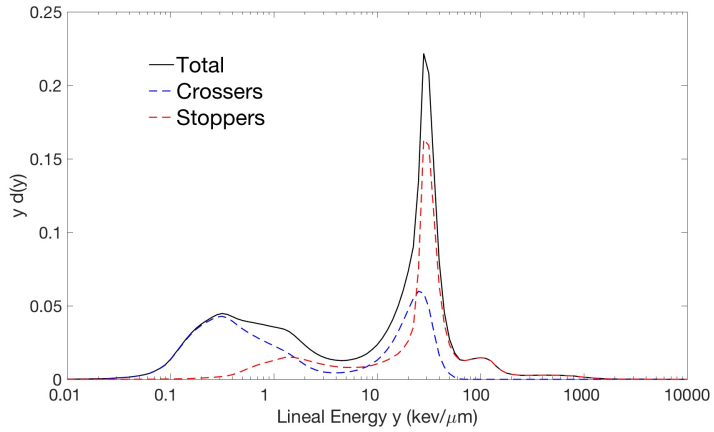

Figure 10: Contribution of stoppers and crossers to the microdosimetric spectrum for the diamond microdosimeter due to an isotropic field of GCR.

5.1. Simulation Study: Charge confinement for cylindrical sensitive volumes

The electric field distribution calculated by the Synopsys TCAD simulation is presented in Fig. 11. The electric field is clearly confined to the cylindrical SV region as defined by the outer electrode structure and boron doped diamond under-layer.

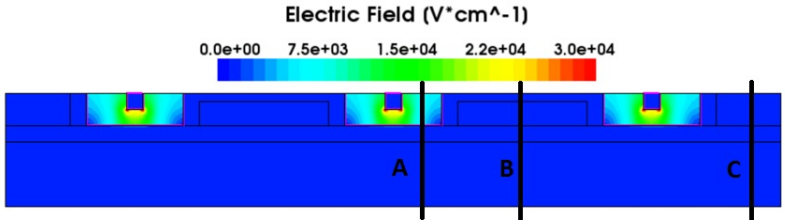

Figure 11: Electric field distribution of the diamond microdosimeter device as derived from Synopsys TCAD. In this work, the device is operated in 'passive' mode, i.e. the inner electrode is under an applied bias of 10 V whilst the outer electrodes of each SV are grounded at 0 V.

The results of the MIP strike charge collection study are presented in Table 4. The simulation shows that charge collection due to ionisation processes was measured only for strikes occurring within the cylindrical SV. In all other cases, the charge collection was so low as to be considered effectively negligible. This study

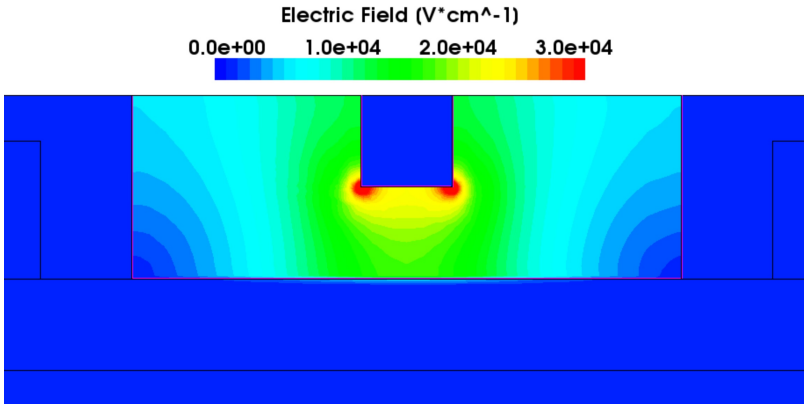

Figure 12: Electric field distribution of the central SV of the diamond microdosimeter depicted in Fig. 11.

confirms the effectiveness of the device design to isolate and confine charge collection to the SV regions and also indicate that cross-talk/charge sharing between SVs will not be an issue. Assuming that this simulated charge confinement translates to a physical realisation of the diamond microdosimeter device, then it is clear that the mean chord length derived from the chord length distribution depicted in Fig. 6 is accurate for isotropic fields and a confirmation of the design concept for microdosimetry in space applications.

Strike Position	**CCE (%)**	**Inside/Outside SV**
A	100	Inside
B	0	Outside
C	0	Outside

Table 4: Relative response in terms of charge collection efficiency as a function of position for ion strikes normally incident upon the diamond microdosimeter. Only strike A which is within the SV has a non-zero charge collection efficiency.

6. Discussion and Conclusion

In this study, the application of a spatially based correction factor to match the microdosimetric spectra and derived average quantities (y_D, y_F and y^*) due to heavy charged particles interacting within a diamond SV (10x10x10 μm^3) to that in a spatially scaled water SV was investigated. A correction factor between 0.32 to 0.33 (equivalent to cubic water SVs with thickness between 30.4 and 30.8μm) was found to be suitable to correct the energy distribution and thus microdosimetric spectra in diamond to that of water for monoenergetic carbon, oxygen, silicon and iron nuclei with energies between 10 $MeV\,u^{-1}$ and 1 $GeV\,u^{-1}$. This is consistent with previous studies restricted to proton and alpha particles. It is therefore reasonable to state that for the energy range of interest, the correction factor is stable and almost independent of the atomic number (Z) of the incident primary particle.

The aforementioned correction factor can be used to geometrically scale the sensitive volumes within diamond based microdosimeters to a water based equivalent structure. A chord length study of diamond and

water SV was performed in order to convert the energy deposition distributions to a microdosimetric spectrum. The mean chord lengths for the diamond and water SVs (C=0.32 and C=0.33) were found to be l_D=11.34µm, l_W=37.28µm (C=0.32) and l_W=36.15µm (C=0.33), respectively. The suitability of this correction factor for diamond based microdosimetry was examined for GCR ions including hydrogen, helium, carbon, oxygen, silicon and iron in the energy range 1 $\mathrm{MeV\,u^{-1}}$ to 100 $\mathrm{GeV\,u^{-1}}$. The agreement between the resulting microdosimetric spectrum was quantified using the KS test. The dose-mean, frequency-mean and saturation-corrected dose-mean lineal energies were also used to provide an alternative figure of merit to assess the agreement between microdosimetric spectrum. The dose-mean lineal energy showed a 1.34% agreement between diamond and water when the correction factor C was equal to 0.32 as compared to 2.88% when the correction factor was 0.33. The saturation-corrected dose-mean lineal energy on the other hand showed better agreement when C=0.33 with a percentage difference of 4.53% as compared to 6.73% when C=0.32. In both cases, i.e. C=0.32 or C=0.33, the percentage difference between the microdosimetric spectrum for diamond and spatially corrected water based microdosimeters was 7.81%. It is clear that the choice of criteria in terms of microdosimetric quantities can have a significant impact upon the determination of agreement between spectrum. Regardless of which measure is used, i.e. the KS test or non-stochastic lineal energies (y_D, y_F and y_*), the agreement between the diamond and water spectrum is deemed acceptable. The study has shown the appropriateness of the correction factor for hadrons typical of the space environment.

The primary peaks within diamond based microdosimeters are the result of proton and alpha energy deposition interactions within the devices. This result is unsurprising as both particles form the primary component (≈99.9 %) of GCR spectra. Events associated with higher lineal energies are the result of the heavier GCR components. Whilst these HZE components only form a small fraction of the entire GCR flux, they can result in significant impact to biological tissue due to the high lineal energies associated with their passage through matter. This work will by extension also be directly applicable for solar particle events (SPE) and heavy ion therapy (HIT), given the particle type and energy range.

This study provides a meaningful tool for the optimisation of detector geometries for microdosimetric application. Whilst the Synopsys TCAD component of this study has shown that the current design is effective in terms of charge confinement and thus SV definition, the Geant4 study has shown that the dimensions of the sensitive volumes should be reduced for microdosimetry. The dimensions of the current prototype microdosimeter modelled in this study is shown to have a significant contribution due to stoppers, i.e., particles which stop within the sensitive volume. In future work, the diamond microdosimeter will be redesigned in order to reduce the probability of stoppers and optimise the design for hadron therapy QA and radioprotection in space. This understanding of the correction factor C will be critical in evaluating future devices and their applicability to represent cellular sized SVs for microdosimetry. Additionally, future work will look at correcting the microdosimetric spectrum from complex convex geometries to spherical geometries in order to perform comparison between diamond based microdosimeters and TEPC.

Acknowledgement

The authors would like to acknowledge the National Computing Infrastructure (NCI), ANFF (Australian National Fabrication Facility) Design House, Multi-modal Australian ScienceS and Visualisation Environment (MASSIVE) M3 cluster and the University of Wollongongs High Performance Cluster for use of their computing facilities. Lastly, the authors acknowledge the funding of ARC Discovery Project grants DP1096600 and DP170102273

References

References

[1] A. J. Tylka, J. H. Adams, P. R. Boberg, B. Brownstein, W. F. Dietrich, E. O. Flueckiger, E. L. Petersen, M. A. Shea, D. F. Smart, E. C. Smith, CREME96 : A Revision of the Cosmic Ray Effects on Micro-Electronics Code, IEEE Transactions on Nuclear Science 44 (6) (1997) 2150–2166.

[2] G. Reitz, R. Beaujean, M. Leicher, Dosimetric measurements in manned missions, Acta Astronautica 36 (8-12) (1995) 517–526. doi:10.1016/0094-5765(95)00137-9.
URL http://www.ncbi.nlm.nih.gov/pubmed/11542777

[3] H. Rossi, M. Zaider, Microdosimetry and its applications, Springer, 1996.

[4] G. F. Knoll, Radiation detection and measurement, 2nd Edition, Wiley, New York, 1989.

[5] Radiation Hazards to Crews of Interplanetary Missions, National Academies Press, Washington, D.C., 1996. doi:10.17226/5540.
URL http://www.nap.edu/catalog/5540

[6] T. Straume, L. A. Braby, T. B. Borak, T. Lusby, D. W. Warner, D. Perez-Nunez, Compact tissue-equivalent proportional counter for deep space human missions, Health Physics 109 (4) (2015) 277–283. doi:10.1097/HP.0000000000000334.

[7] S. Agosteo, G. A. P. Cirrone, P. Colautti, G. Cuttone, G. D'Angelo, A. Fazzi, M. V. Introini, D. Moro, A. Pola, V. Varoli, Study of a silicon telescope for solid state microdosimetry: Preliminary measurements at the therapeutic proton beam line of CATANA, Radiation Measurements 45 (10) (2010) 1284–1289. doi:10.1016/j.radmeas.2010.06.051.
URL http://dx.doi.org/10.1016/j.radmeas.2010.06.051

[8] S. Agosteo, A. Fazzi, M. V. Introini, M. Lorenzoli, A. Pola, A telescope detection system for direct and high resolution spectrometry of intense neutron fields, Radiation Measurements 85 (2016) 1–17. doi:10.1016/j.radmeas.2015.12.005.
URL http://dx.doi.org/10.1016/j.radmeas.2015.12.005

[9] P. Colautti, V. Conte, A. Selva, S. Chiriotti, A. Pola, D. Bortot, A. Fazzi, S. Agosteo, M. Ciocca, MICRODOSIMETRIC STUDY AT THE CNAO ACTIVE-SCANNING CARBON-ION BEAM, Radiation Protection Dosimetry (June) (2017) 1–5. doi:10.1093/rpd/ncx217.
URL http://academic.oup.com/rpd/article/doi/10.1093/rpd/ncx217/4565819/MICRODOSIMETRIC-STUDY-AT-THE-CNAO-ACTIVESCANNING

[10] L. T. Tran, L. Chartier, D. A. Prokopovich, M. I. Reinhard, M. Petasecca, S. Guatelli, M. L. F. Lerch, V. L. Perevertaylo, M. Zaider, N. Matsufuji, M. Jackson, M. Nancarrow, A. B. Rosenfeld, 3D-Mesa "Bridge" Silicon Microdosimeter: Charge Collection Study and Application to RBE Studies in Radiation Therapy, IEEE Transactions on Nuclear Science 62 (2) (2015) 504–511.

[11] L. T. Tran, L. Chartier, D. A. Prokopovich, D. Bolst, M. Povoli, A. Summanwar, A. Kok, A. Pogossov, M. Petasecca, S. Guatelli, M. I. Reinhard, M. Lerch, M. Nancarrow, N. Matsufuji, M. Jackson, A. B. Rosenfeld, Thin Silicon Microdosimeter Utilizing 3-D MEMS Fabrication Technology: Charge Collection Study and Its Application in Mixed Radiation Fields, IEEE Transactions on Nuclear Science 65 (1) (2018) 467–472. doi:10.1109/TNS.2017.2768062.
URL http://ieeexplore.ieee.org/document/8089762/

[12] D. Bolst, S. Guatelli, L. T. Tran, L. Chartier, M. L. Lerch, N. Matsufuji, A. B. Rosenfeld, Correction factors to convert microdosimetry measurements in silicon to tissue in 12C ion therapy, Physics in Medicine and Biology 62 (6) (2017) 2055–2069. doi:10.1088/1361-6560/aa5de5.

[13] L. T. Tran, L. Chartier, D. Bolst, J. A. Davis, D. A. Prokopovich, A. Pogossov, S. Guatelli, M. I. Reinhard, M. Petasecca, M. L. F. Lerch, N. Matsufuji, M. Povoli, A. Summanwar, A. Kok, M. Jackson, A. B. Rosenfeld, In-field and out-of-file application in 12C ion therapy using fully 3D silicon microdosimeters, Radiation Measurements.

[14] T. Kashiwagi, K. Hibino, H. Kitamura, K. Mori, S. Okuno, T. Takashima, Y. Uchihori, K. Yajima, M. Yokota, K. Yoshida, Investigation of basic characteristics of synthetic diamond radiation detectors, IEEE Transactions on Nuclear Science 53 (2) (2006) 630–635. doi:10.1109/TNS.2006.871505.
URL http://ieeexplore.ieee.org/document/1621376/

[15] ICRU, Fundamental quantities and units for ionizing radiation (ICRU Report 85), J.ICRU 11 (2011) 1–31.

[16] F. H. Attix, Introduction to Radiological Physics and Radiation Dosimetry, Wiley, New York, 1986.

[17] J. A. Davis, S. Guatelli, M. Petasecca, M. L. F. Lerch, M. I. Reinhard, M. Zaider, J. Ziegler, A. B. Rosenfeld, Tissue Equivalence Study of a Novel Diamond-Based Microdosimeter for Galactic Cosmic Rays and Solar Particle Events, IEEE Transactions on Nuclear Science 61 (4) (2014) 1544–1551. doi:10.1109/TNS.2014.2298032.
URL http://ieeexplore.ieee.org/lpdocs/epic03/wrapper.htm?arnumber=6742631

[18] National Institutes of Standards and Technology.
URL http://www.nist.gov/

[19] M. Berger, J. Coursey, M. Zucker, J. Change, ESTAR, PSTAR, and ASTAR: Computer Programs for Calculating Stopping-Power and Range Tables for Electrons, Protons, and Helium Ions (version 1.2.3). (2005).
URL http://www.nist.gov/pml/data/star/index.cfm

[20] J. A. Davis, K. Ganesan, D. A. Prokopovich, M. Petasecca, M. L. F. Lerch, D. N. Jamieson, A. B. Rosenfeld, A 3D lateral electrode structure for diamond based microdosimetry, Applied Physics Letters 110 (1) (2017) 013503. doi:10.1063/1.4973628.
URL http://aip.scitation.org/doi/10.1063/1.4973628http://dx.doi.org/10.1063/1.4973628

[21] S. Agostinelli, J. Allison, K. Amako, J. Apostolakis, H. Araujo, P. Arce, M. Asai, D. Axen, S. Banerjee, G. Barrand, F. Behner, L. Bellagamba, J. Boudreau, L. Broglia, A. Brunengo, H. Burkhardt, S. Chauvie, J. Chuma, R. Chytracek, G. Cooperman, G. Cosmo, P. Degtyarenko, A. Dell'Acqua, G. Depaola, D. Dietrich, R. Enami, A. Feliciello, C. Ferguson, H. Fesefeldt, G. Folger, F. Foppiano, A. Forti, S. Garelli, S. Giani, R. Giannitrapani, D. Gibin, J. J. Gomez Cadenas, I. Gonzalez, G. Gracia Abril, G. Greeniaus, W. Greiner, V. Grichine, A. Grossheim, S. Guatelli, P. Gumplinger, R. Hamatsu, K. Hashimoto, H. Hasui, A. Heikkinen, A. Howard, V. Ivanchenko, A. Johnson, F. W. Jones, J. Kallenbach, N. Kanaya, M. Kawabata, Y. Kawabata, M. Kawaguti, S. Kelner, P. Kent, A. Kimura, T. Kodama, R. Kokoulin, M. Kossov, H. Kurashige, E. Lamanna, T. Lampen, V. Lara, V. Lefebure, F. Lei,

M. Liendl, W. Lockman, F. Longo, S. Magni, M. Maire, E. Medernach, K. Minamimoto, P. Mora de Freitas, Y. Morita, K. Murakami, M. Nagamatu, R. Nartallo, P. Nieminen, T. Nishimura, K. Ohtsubo, M. Okamura, S. O'Neale, Y. Oohata, K. Paech, J. Perl, A. Pfeiffer, M. G. Pia, F. Ranjard, A. Rybin, S. Sadilov, E. di Salvo, G. Santin, T. Sasaki, N. Savvas, Y. Sawada, S. Scherer, S. Sei, V. Sirotenko, D. Smith, N. Starkov, H. Stoecker, J. Sulkimo, M. Takahata, S. Tanaka, E. Tcherniaev, E. Safai Tehrani, M. Tropeano, P. Truscott, H. Uno, L. Urban, P. Urban, M. Verderi, A. Walkden, W. Wander, H. Weber, J. P. Wellisch, T. Wenaus, D. C. Williams, D. Wright, T. Yamada, H. Yoshida, D. Zschiesche, GEANT4 - A simulation toolkit, Nuclear Instruments and Methods in Physics Research, Section A: Accelerators, Spectrometers, Detectors and Associated Equipment 506 (3) (2003) 250–303. arXiv:1005.0727v1, doi:10.1016/S0168-9002(03)01368-8.

[22] J. Allison, K. Amako, J. Apostolakis, H. Araujo, P. A. Dubois, M. Asai, G. Barrand, R. Capra, S. Chauvie, R. Chytracek, G. A. P. Cirrone, G. Cooperman, G. Cosmo, G. Cuttone, G. G. Daquino, M. Donszelmann, M. Dressel, G. Folger, F. Foppiano, J. Generowicz, V. Grichine, S. Guatelli, P. Gumplinger, A. Heikkinen, I. Hrivnacova, A. Howard, S. Incerti, V. Ivanchenko, T. Johnson, F. Jones, T. Koi, R. Kokoulin, M. Kossov, H. Kurashige, V. Lara, S. Larsson, F. Lei, O. Link, F. Longo, M. Maire, A. Mantero, B. Mascialino, I. Mclaren, P. M. Lorenzo, K. Minamimoto, K. Murakami, P. Nieminen, L. Pandola, S. Parlati, L. Peralta, J. Perl, A. Pfeiffer, M. G. Pia, A. Ribon, P. Rodrigues, G. Russo, S. Sadilov, G. Santin, T. Sasaki, D. Smith, N. Starkov, S. Tanaka, E. Tcherniaev, B. Tomé, A. Trindade, P. Truscott, L. Urban, M. Verderi, A. Walkden, J. P. Wellisch, D. C. Williams, D. Wright, H. Yoshida, Geant4 Developments and Applications, IEEE Transactions on Nuclear Science 53 (1) (2006) 270–278.

[23] S. Chauvie, Z. Francis, S. Guatelli, S. Incerti, B. Mascialino, P. Moretto, P. Nieminen, M. G. Pia, Geant4 Physics Processes for Microdosimetry Simulation : Design Foundation and Implementation of the First Set of Models 54 (6) (2007) 2619–2628.

[24] K. Amako, S. Guatelli, V. Ivanchenko, M. Maire, B. Mascialino, K. Murakami, P. Nieminen, L. Pandola, S. Parlati, M. Pia, M. Piergentili, T. Sasaki, L. Urban, Comparison of Geant4 electromagnetic physics models against the NIST reference data, IEEE Transactions on Nuclear Science 52 (4) (2005) 910–918. doi:10.1109/TNS.2005.852691.
URL http://ieeexplore.ieee.org/lpdocs/epic03/wrapper.htm?arnumber=1495783

[25] MathsWorks Inc, Matlab (1998).

[26] N. Smirnov, Table for Estimating the Goodness of Fit of Empirical Distributions, The Annals of mathematical statistics 19 (2) (1948) 279–281. doi:10.1214/aoms/1177730256.
URL http://projecteuclid.org/euclid.aoms/1177730256

[27] I. A. Zahradnik, M. T. Pomorski, L. De Marzi, D. Tromson, P. Barberet, N. Skukan, P. Bergonzo, G. Devès, J. Herault, W. Kada, T. Pourcher, S. Saada, scCVD Diamond Membrane based Microdosimeter for Hadron Therapy, Physica Status Solidi (A) Applications and Materials Science 215 (22) (2018) 1–10. doi:10.1002/pssa.201800383.

[28] S. J. Rashid, S. Member, A. Tajani, D. J. Twitchen, L. Coulbeck, F. Udrea, T. Butler, N. L. Rupesinghe, M. Brezeanu, J. Isberg, a. Garraway, M. Dixon, R. S. Balmer, D. Chamund, P. Taylor, G. a. J. Amaratunga, A. High-quality, Numerical Parameterization of Diamond for Device Simulation and Analysis, Ieee Transactions on Electron Devices 55 (10) (2008) 2744–2756.

[29] M. Brezeanu, T. Butler, N. Rupesinghe, S. Rashid, M. Avram, G. Amaratunga, F. Udrea, M. Dixon, D. Twitchen, A. Garraway, D. Chamund, P. Taylor, Single crystal diamond MiP diodes for power electronics, IET Circuits, Devices & Systems 1 (5) (2007) 380. doi:10.1049/iet-cds:20060379. URL http://digital-library.theiet.org/content/journals/10.1049/iet-cds{_}20060379

[30] A. Morozzi, D. Passeri, K. Kanxheri, L. Servoli, S. Lagomarsino, S. Sciortino, Polycrystalline CVD diamond device level modeling for particle detection applications, Journal of Instrumentation 11 (12). doi:10.1088/1748-0221/11/12/C12043.